Controlling Vector Bessel Beams with Metasurfaces

Carl Pfeiffer and Anthony Grbic*

Department of Electrical Engineering and Computer Science, University of Michigan, Ann Arbor, Michigan 48109-2122, USA

(Received 16 July 2014; published 23 October 2014)

Unprecedented control of an electromagnetic wave front is demonstrated with reflectionless metasurfaces that can manipulate vector Bessel beams: cylindrical vector beams with a Bessel profile. First, two metasurfaces are developed to convert linearly and circularly polarized Gaussian beams into vector Bessel beams. Each unit cell of the metasurfaces provides polarization and phase control with high efficiency. Next, the reciprocal process is demonstrated: an incident radially polarized Bessel beam is transformed into collimated, linearly and circularly polarized beams. In this configuration, a planar Bessel beam launcher is integrated with a collimating metasurface lens to realize a low-profile lens-antenna. The lens-antenna achieves a high directivity (exceeding 20 dB) with a subwavelength overall thickness. Finally, a metasurface providing isotropic polarization rotation is used to transform a radially polarized Bessel beam into an azimuthally polarized Bessel beam. This work demonstrates that metasurfaces can be used to generate arbitrary combinations of radial and azimuthal polarizations for applications such as focus shaping or generating tractor beams.

DOI: 10.1103/PhysRevApplied.2.044012

I. INTRODUCTION

Vector Bessel beams play a critical role in many optical systems [1]. These beams maintain a high-intensity focus over a considerable distance for applications such as particle trapping, tractor beams, near-field probes, laser machining, lithography, and optical data storage [2–4]. In addition, their azimuthal and radial polarizations are useful for the spectroscopy of magnetic dipole transitions in quantum dots [5]. Such beams also provide information about the orientation of a single molecule and are ideal sources for exciting surface plasmons in axially symmetric structures [5,6]. Therefore, developing a simple means of transforming a commonplace Gaussian beam into a vector Bessel beam is highly desirable. However, this transformation requires both polarization and phase control, which typically involve multiple lenses, spatial light modulators, dielectric wave plates, or other bulky components [1,6,7].

Recently, ultrathin metasurfaces have shown great promise for controlling electromagnetic wave fronts [8,9]. Metasurfaces are the two-dimensional equivalent of metamaterials and receive much attention, since they can offer reduced losses, are lower profile, and are simpler to fabricate than bulk metamaterials [10]. Single-layer metasurfaces with resonant geometries, such as V antennas, are used to control optical wave fronts [11–13]. However, such metasurfaces possess only an electric response. This response results in significant reflection, since electric dipoles are bidirectional radiators [14]. In addition, only a single component of the polarization can be manipulated, which severely limits polarization control. Realizing a vector Bessel beam requires both polarization and phase control, which introduce added challenges. To date, limited control of both polarization and phase has been demonstrated. However, the reported structures typically suffer from low efficiencies, since their impedance is mismatched to free space [15].

In this work, two metasurfaces are introduced to efficiently convert normally incident Gaussian beams into Bessel beams. The first metasurface transforms x- and y-polarized Gaussian beams into transverse magnetic (TM or radially polarized) and transverse electric (TE or azimuthally polarized) polarized Bessel beams, respectively. The second metasurface transforms an incident left-handed-circularly-polarized Gaussian beam into a transmitted TM-polarized Bessel beam, as shown in Fig. 1. Correspondingly, the two metasurfaces will be referred to as the linear-to-Bessel and the circular-to-Bessel metasurfaces. The unit cells comprising both metasurfaces utilize three anisotropic sheet admittances cascaded along the direction of propagation ($\hat{z}$). The cells are individually designed to realize a stipulated phase shift along their respective spatially varying principal axes while at the same time maintaining high transmission. Thus, the metasurfaces are low loss and impedance matched to free space to maximize efficiency.

Next, the reciprocal process is demonstrated: a TM-polarized Bessel beam is transformed into a collimated beam. In addition to providing further experimental verification, this configuration is used to develop a low-profile lens-antenna. The lens-antenna combines a planar Bessel beam launcher with collimating lenses (the proposed

*To whom correspondence should be addressed.
agrbic@umich.edu

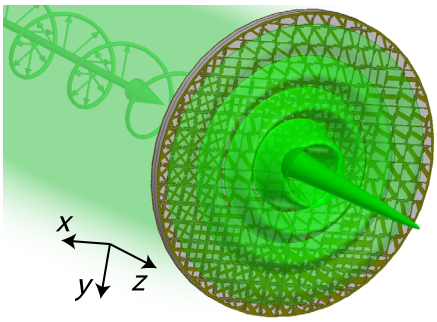

FIG. 1. An inhomogeneous, anisotropic metasurface transforms a circularly polarized Gaussian beam into a vector Bessel beam with high efficiency.

metasurfaces). This low-profile lens-antenna has a subwavelength overall thickness to realize a high directivity (exceeding 20 dB). The design achieves an order-of-magnitude size reduction over previously reported lens-antenna [16]. Finally, a metasurface providing polarization rotation (polarization rotator) is placed directly above the Bessel beam launcher to transform the incident TM-polarized Bessel beam into a transmitted TE-polarized Bessel beam. This polarization rotator is isotropic and rotates any linear electric field polarization by $\pi/2$. In the future, metasurfaces providing a polarization rotation of angles less extreme than $\pi/2$ can be used for exciting arbitrary combinations of TM and TE polarizations for focus shaping or generating tractor beams [2,17].

II. REVIEW OF VECTOR BESSEL BEAMS

Vector Bessel beams are axially symmetric beam solutions to Maxwell's equations [18,19]. They can be written as

$$\begin{aligned}\mathbf{E} &= e^{-jk_z z}\left(C_{\mathrm{TM}}J_0(k_\rho\rho)\hat{\mathbf{z}} - C_{\mathrm{TE}}\frac{k\eta}{k_\rho}jJ_1(k_\rho\rho)\hat{\boldsymbol{\phi}}\right.\\ &\quad\left.+C_{\mathrm{TM}}\frac{k_z}{k_\rho}jJ_1(k_\rho\rho)\hat{\boldsymbol{\rho}}\right),\\ \mathbf{H} &= e^{-jk_z z}\left(C_{\mathrm{TE}}J_0(k_\rho\rho)\hat{\mathbf{z}} + C_{\mathrm{TM}}\frac{k}{\eta k_\rho}jJ_1(k_\rho\rho)\hat{\boldsymbol{\phi}}\right.\\ &\quad\left.+C_{\mathrm{TE}}\frac{k_z}{k_\rho}jJ_1(k_\rho\rho)\hat{\boldsymbol{\rho}}\right),\end{aligned} \tag{1}$$

where C_{TM} and C_{TE} represent the coefficients of the TM- (radially) and TE- (azimuthally) polarized Bessel beams, respectively. A time-harmonic progression of $e^{j\omega t}$ and propagation in the $\hat{\mathbf{z}}$ direction is assumed. In Eq. (1), k_ρ and k_z are the transverse and longitudinal wave numbers, respectively, which satisfy the separation relation $k_z^2 + k_\rho^2 = k^2 = \omega^2\epsilon\mu$, and $J_0(k_\rho\rho)$ and $J_1(k_\rho\rho)$ are the zeroth- and first-order Bessel functions of the first kind. Nonparaxial Bessel beams with transverse wave numbers of $k_\rho = 0.8k$ are chosen in this study. The Bessel beams under consideration are truncated with a Gaussian windowing function $[\exp(-\rho^2/w_0^2)]$. Hence, these beams are often referred to as Bessel-Gauss beams.

III. METASURFACE DESIGN

It is well known how to transform linear or circular polarization to cylindrical polarization by using the Jones matrices of spatially varying wave plates [6,20,21]. In short, each unit cell of the linear-to-Bessel metasurface acts as a half-wave plate, and each unit cell of the circular-to-Bessel metasurface acts as a quarter-wave plate. Such configurations allow the polarization to be transformed from linear and circular, respectively, to cylindrical. In addition, the metasurfaces must apply an inhomogeneous phase shift across their surfaces to transform the wave front from a Gaussian profile to a Bessel profile. The necessary phase shift provided by each unit cell is determined by simply subtracting the phase of the desired wave front (Bessel beam) from the phase of the incident wave front (Gaussian beam). Figure 2 shows the slow axis of each unit cell and the phase shift that should be imparted by the fast axis of the metasurface. For clarity, only the middle portion of the metasurfaces is shown. Note that the circular-to-Bessel metasurface requires quarter-wave plates whose fast axis provides a full 2π phase coverage. This property should not be confused with earlier metasurfaces that provided complete phase control for circularly polarized light by local changes in the polarization (Pancharatnam-Berry phase) [22]. Additional design details are provided in Supplemental Material [23].

The geometry shown in Fig. 3(a) is employed to realize the unit cells of the metasurfaces. It consists of patterned metallic sheets (sheet admittances) cascaded in the direction of propagation. The metallic patterns are separated by Rogers 4003 substrates ($\epsilon_r = 3.55$ and $\tan\delta = 0.0027$) that are 1.52 mm ($\lambda/19.7$) in thickness. Provided the overall thickness of the cascaded metallic and dielectric substrates is subwavelength, this structure is well modeled as a single metasurface boundary condition [10]. It has been shown that this structure can realize complete control of the transmitted phase while maintaining near-unity transmittance [24,25]. In addition, utilizing anisotropic sheets allows for polarization control [26]. However, in these previous structures, there is no experimental demonstration of wave-front control along two dimensions. Furthermore, the principal axes of every unit cell are aligned along the x and y axes, which limits the degree to which the polarization could be controlled. Here, it is experimentally demonstrated that wave fronts with arbitrary (spatially varying) phase and polarization profiles can be generated.

A typical unit cell of the linear-to-Bessel metasurface is shown in Fig. 3(b). Each sheet admittance of a unit cell can be modeled as a parallel LC circuit. The inductance results from the metallic grid outlining the cell, and the

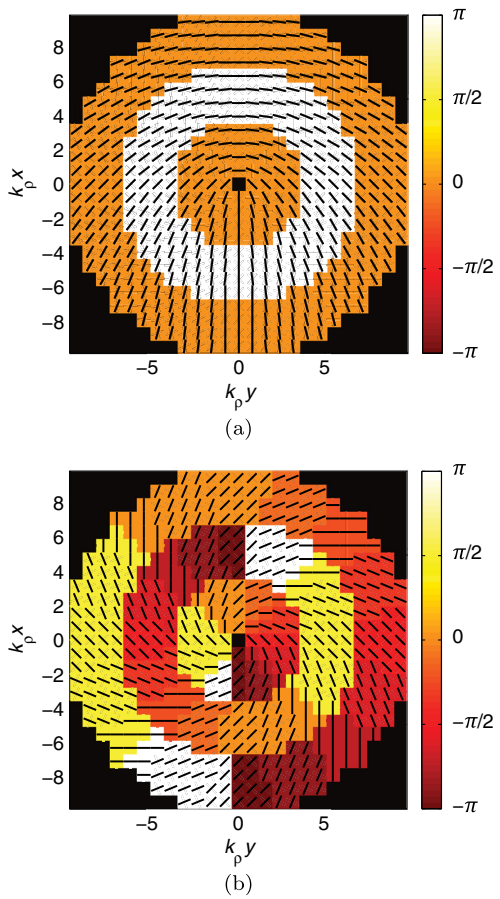

FIG. 2. (a) Designed metasurface that converts a linearly polarized Gaussian beam into a vector Bessel beam. Each unit cell acts as a half-wave plate. When the incident polarization of the Gaussian beam is oriented along $\hat{\boldsymbol{x}}$ and $\hat{\boldsymbol{y}}$, the transmitted Bessel beam is TM and TE polarized, respectively. (b) Designed metasurface that converts a circularly polarized Gaussian beam into a TM-polarized Bessel beam. Each unit cell acts as a quarter-wave plate. For both plots, the lines and color correspond to the orientation of the slow axis and the phase shift of the fast axis, respectively.

capacitance from the top-hat loaded crossed dipole at the center. Each sheet admittance can be controlled by adjusting the dimensions and orientation of the crossed dipole relative to the x axis. An additional advantage of this geometry is that the metallic grid outlining the unit cell reduces undesired coupling between neighboring unit cells, which is inherent to inhomogeneous designs such as this [24]. The average simulated transmittances of the fast and slow axes of all unit cells comprising the linear-to-Bessel metasurface are 0.93 and 0.84, respectively. The average simulated transmittances of the fast and slow axes of all unit cells comprising the circular-to-Bessel metasurface are 0.80 and 0.79, respectively. This high transmittance demonstrates that both metasurface designs exhibit low loss and are impedance matched to free space. Additional design details are provided in Supplemental Material [23].

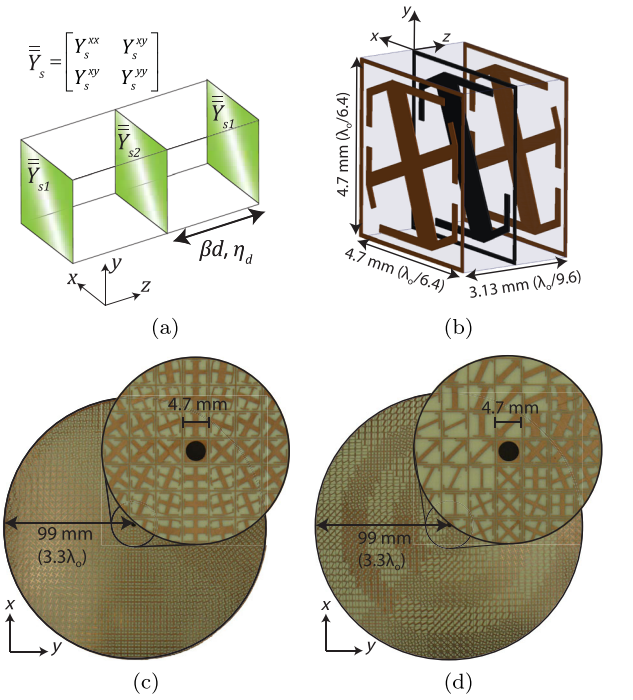

FIG. 3. (a) Analytic model used to design each unit cell. (b) Schematic of a typical unit cell. This particular cell acts as a half-wave plate with its fast axis oriented along $\phi = -\pi/8$. (c) Fabricated metasurface that converts a linearly polarized Gaussian beam into a vector Bessel beam. (d) Fabricated metasurface that converts a circularly polarized Gaussian beam into a TM-polarized Bessel beam.

IV. GENERATING BESSEL BEAMS

The metasurfaces are fabricated by using standard printed-circuit-board processes. The top layers are shown in Figs. 3(c) and 3(d). Both metasurfaces have an operating frequency of 9.9 GHz, a radius of 99 mm (3.3λ), and an overall thickness of 3.13 mm $(\lambda/9.6)$. They are experimentally characterized by illuminating them with a Gaussian beam [27]. The transmitted fields are scanned at a distance $z = 15$ mm from the surface. The normally incident Gaussian beam had a beam waist radius of $w_0 = 57$ mm (1.9λ). The experimental setup is identical to that described in Ref. [14], and additional measurement details are provided in Supplemental Material [23].

First, the linear-to-Bessel metasurface is illuminated with x- and y-polarized electric fields, and the transmitted tangential magnetic field is measured, as shown in Figs. 4(a) and 4(b). When illuminated with x and y polarization, the transmitted magnetic field is polarized along $\hat{\boldsymbol{\phi}}$ and $\hat{\boldsymbol{\rho}}$, respectively. Note that radially (TM-) and azimuthally (TE-) polarized Bessel beams have tangential magnetic fields that are polarized in the $\hat{\boldsymbol{\phi}}$ and $\hat{\boldsymbol{\rho}}$ directions, as given by Eq. (1). The nondiffracting property of the TM-polarized Bessel beam is also verified by measuring the longitudinal electric field, as shown in Fig. 4(c). It can be

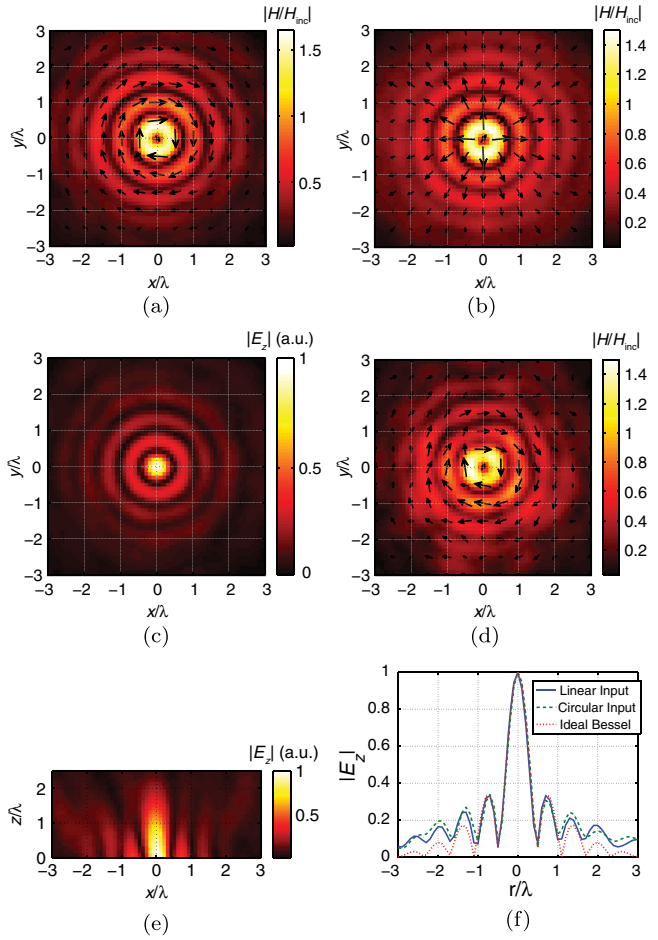

FIG. 4. Measurements of the fabricated metasurfaces at the operating frequency of 9.9 GHz. For all plots, the arrows point in the direction of the magnetic field, and the color corresponds to the absolute value of the magnetic or electric fields. (a),(b) Transmitted magnetic field when x- and y-polarized Gaussian beams are incident on the linear-to-Bessel metasurface, respectively. (c) Transmitted z-directed electric field when an x-polarized Gaussian beam is incident upon the linear-to-Bessel metasurface. (d),(e) Transmitted magnetic field in the xy plane and z-directed electric field in the xz plane, respectively, when a $\hat{\boldsymbol{z}}$-propagating, left-handed-circularly-polarized Gaussian beams is incident on the circular-to-Bessel metasurface. (f) Profile of the transmitted wave front when x-polarized and left-handed-circular-polarized Gaussian beams are incident upon the linear-to-Bessel and circular-to-Bessel metasurfaces, respectively. In addition, an ideal Gaussian truncated Bessel pattern is plotted as a reference.

seen that the electric field closely resembles a zeroth-order Bessel function, as expected.

Next, the circular-to-Bessel metasurface is characterized. As shown in Fig. 4(d), a left-handed-circular polarization incident on the circular-to-Bessel metasurface results in a TM-polarized Bessel beam, as evidenced by the $\hat{\boldsymbol{\phi}}$-directed magnetic field. In addition, Fig. 4(e) shows that the Bessel beam propagates a considerable distance from the metasurface located at the $z = 0$ plane. It should be noted that, if the incident Gaussian beam were to travel in the $-\hat{\boldsymbol{z}}$ direction rather than the $+\hat{\boldsymbol{z}}$ direction, the circular-to-Bessel metasurface would instead convert right-handed-circular polarization into the TM polarization. Figure 4(f) plots the profile of the transmitted wave front for the cases where an x-polarized field is incident upon the linear-to-Bessel metasurface and a left-handed-circular-polarized field is incident upon the circular-to-Bessel metasurface. In addition, an ideal Bessel-Gauss pattern $[J_0(k_\rho\rho)\exp(-\rho^2/w_0^2)]$ is plotted as a reference.

V. COLLIMATING BESSEL BEAMS

Thus far, two different metasurfaces are reported that show efficient polarization and wave-front control. The metasurfaces transform a collimated beam (Gaussian beam) into a Bessel beam. The performance of the metasurfaces can be further verified by operation in a reciprocal manner: transforming an incident TM-polarized Bessel beam into a collimated beam. In this configuration, a planar Bessel beam launcher is integrated with the two developed metasurface lenses to realize low-profile lens-antennas. The Bessel beam launcher presented in Refs. [28,29] radiates a TM-polarized Bessel beam just above its surface. The linear-to-Bessel and circular-to-Bessel metasurfaces are placed a subwavelength distance from the launcher to collimate the radiation and convert the polarization from radial to linear or circular, respectively [see Fig. 5(a)]. A 4-mm-thick foam spacer composed of Rohacell 31 HF ($\epsilon_r = 1.046$ and $\tan\delta = 0.0017$) is used to separate the metasurfaces from the Bessel beam launcher. The Bessel beam launcher generates a TM-polarized Bessel beam by using a leaky radial waveguide whose thickness is deeply subwavelength ($\lambda/50$). Outward- and inward-propagating Hankel functions within the radial waveguide interfere to produce a Bessel beam. The gain of the Bessel beam launcher alone is measured to be 5.2 dB at the operating frequency of 9.9 GHz, and its radiation pattern is shown in Fig. 5(b) [30]. The experimental setup of the Bessel beam launcher and metasurface lens combination is shown in Fig. 5(c).

Figures 5(d) and 5(e) show the radiation patterns when the linear-to-Bessel and circular-to-Bessel metasurfaces are placed 4 mm ($\lambda/7.5$) from the Bessel beam launcher, respectively. The radiation generated by the Bessel beam launcher is collimated by the metasurfaces to the broadside direction. The gains of the linear and circular lens-antennas are measured to be 22.1 and 20.4 dB, respectively, at the operating frequency. Both lens-antennas exhibited a cross-polarization level of less than -20 dB relative to the copolarized radiation in the direction of the main beam. The half-power gain bandwidths are measured to be 8.1% and 7.6% for linear and circular polarizations, respectively. The overall thickness of the Bessel beam launcher and metasurface lens combination is 7.7 mm ($\lambda/3.9$). In comparison, a typical lens-antenna system places an elementary source

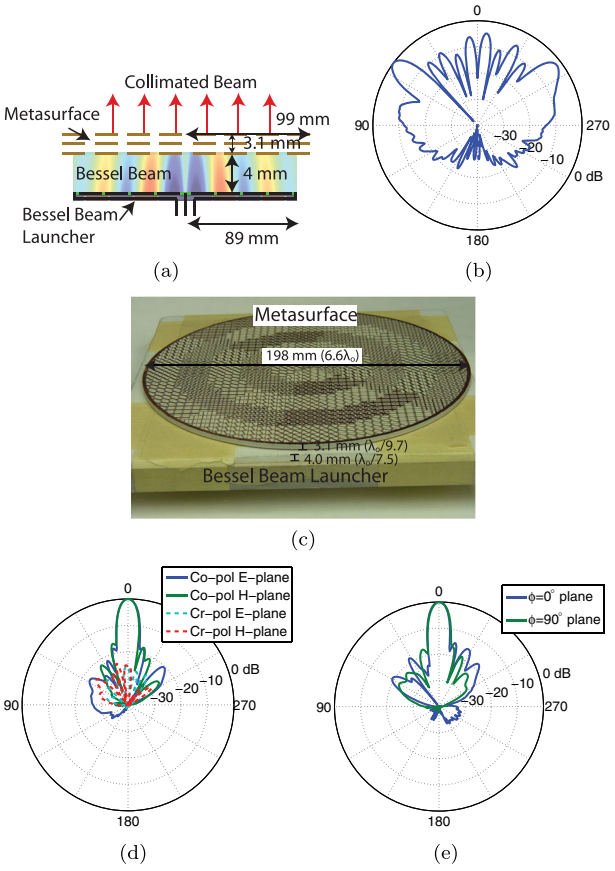

FIG. 5. Transforming a Bessel beam into a highly collimated beam. (a) Schematic of the Bessel beam generation and its conversion to a collimated beam. (b) Measured radiation pattern of the Bessel beam launcher. (c) Experimental setup of the circular-to-Bessel metasurface placed on top of the Bessel beam launcher. A 4-mm Rohacell 31 HF foam spacer separates the Bessel beam launcher and the metasurface. (d) Measured radiation pattern of the Bessel beam launcher with the linear-to-Bessel metasurface placed on top. (e) Measured radiation pattern of the Bessel beam launcher with the circular-to-Bessel metasurface placed on top.

(e.g., low-gain horn antenna) at a significant distance (multiple wavelengths) from a lens. This distance allows the fields to spread out so that a large beam size (or, equivalently, a high directivity) can be realized. Previous lens-antenna systems have overall thicknesses that are larger than the lens radius (99 mm) to realize similar gains [16]. Thus, the proposed lens-antenna design has an order-of-magnitude size reduction over the state of the art. It should be noted that traveling-wave antennas utilizing radial line slots [31,32], partially reflecting surfaces [33], fast-wave structures [34], and modulated surface impedances [35] can also generate highly directive radiation with a planar structure. However, these antennas often have prohibitively narrow operating bandwidths [33] and require time-consuming optimization techniques during design [32].

VI. TRANSFORMING THE POLARIZATION OF BESSEL BEAMS

In addition to the two metasurfaces that generate and collimate vector Bessel beams, an isotropic and homogeneous metasurface that converts the polarization from TM to TE (and vice versa) is developed. This metasurface is referred to as a polarization rotator, because it rotates any linearly polarized wave front by $\pi/2$ [36]. In contrast, a half-wave plate rotates the polarization by $\pi/2$ only when the incident linear polarization is oriented at $\pi/4$ relative to the principal axes of the wave plate. To demonstrate cylindrical polarization conversion, the polarization rotator shown in Fig. 6 is placed 4 mm from the Bessel beam launcher to convert the polarization from TM to TE. This experiment provides excellent verification of the metasurface, since a TM polarization contains spatially varying linear polarizations of all orientations.

Similar to the linear-to-Bessel and circular-to-Bessel metasurfaces, the polarization rotator consists of cascaded metallic sheets, as shown in Fig. 6(b). However, the principal axes of each sheet comprising the polarization

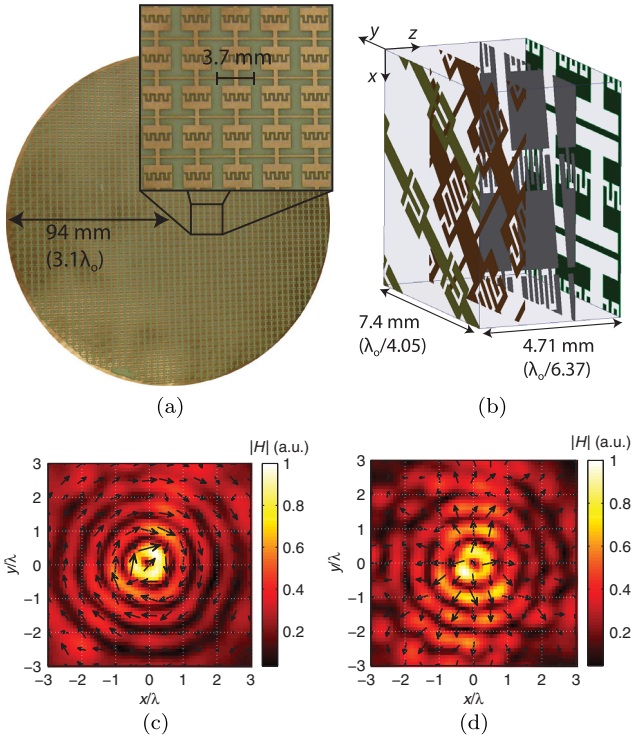

FIG. 6. Transforming a TM-polarized Bessel beam into a TE-polarized Bessel beam by using a polarization rotator. (a) Bottom side of the fabricated polarization rotator. (b) Schematic of a section of the polarization rotator. (c) Measured magnetic field radiated by the Bessel beam launcher. (d) Measured magnetic field after the polarization rotator is placed 4 mm from the Bessel beam launcher. Again, the arrows point in the direction of the magnetic field, and the color corresponds to the absolute value of the magnetic field.

rotator are rotated with respect to the others. This rotation gives the metasurface a significant chiral response, which is necessary to achieve isotropic polarization rotation [36]. In addition, the polarization rotator is homogeneous, which has the advantage that only a single unit cell needs to be designed. The polarization rotator is designed to operate at 10 GHz, but fabrication tolerances shift the operating frequency to 9.8 GHz. Figure 6(c) shows the magnetic field radiated by the Bessel beam launcher, and Fig. 6(d) shows the field after the polarization rotator is placed on top. The field is efficiently converted from TM to TE by the polarization rotator.

VII. SUMMARY

This work extends the capabilities of metasurfaces to enable highly efficient polarization and phase control of a wave front. This result is demonstrated with two different metasurfaces that transform linearly and circularly polarized Gaussian beams to vector Bessel beams. In addition, the metasurfaces are operated in a reciprocal manner. They are combined with a planar Bessel beam launcher to realize a lens-antenna with a subwavelength overall thickness that achieves a high directivity. Finally, an isotropic polarization rotator is used to convert a cylindrical polarization from radial to azimuthal.

Inhomogeneous and anisotropic metasurfaces that provide extreme wave-front control are considered here. In the future, a bianisotropic response could be added to allow for additional polarization control [36]. For example, it is shown that the linear-to-Bessel metasurface generates radial polarization when illuminated with x polarization and azimuthal polarization when illuminated with y polarization. In contrast, it can be shown that the circular-to-Bessel metasurface requires an additional chiral response in order to achieve the same effect with incident right-handed-circular and left-handed-circular polarizations. In addition, the lens-antenna can be further optimized by incorporating other leaky-wave or surface-wave feeding structures to replace the Bessel beam launcher [37–39]. This optimization would enable amplitude control as well as phase and polarization control. In addition, this work can be extended to infrared and visible wavelengths [40,41], which could enable a myriad of compact nanophotonic devices. In particular, it should be possible to realize tractor beams composed of both TM- and TE-polarized Bessel beams, from incident Gaussian beams [2].

ACKNOWLEDGMENTS

The authors thank M. Ettorre and S. M. Rudolph for designing and fabricating the Bessel beam launcher. The authors also acknowledge helpful discussions with Dr. Nicholaos Limberopoulos and Dr. Boris Tomasic from the Sensors Directorate, Air Force Research Laboratory. This work is supported by the Air Force Research Laboratory through the Advanced Materials, Manufacturing and Testing Information Analysis Center (AMMTIAC) contract with Alion Science and Technology, Contract No. FA4600-060D003, the National Science Foundation Materials Research Science and Engineering Center program DMR 1120923 (Center for Photonics and Multiscale Nanomaterials at the University of Michigan), and a Presidential Early Career Award for Scientists and Engineers No. FA9550-09-1-0696.

[1] D. McGloin and K. Dholakia, Bessel beams: Diffraction in a new light, Contemp. Phys. **46**, 15 (2005).
[2] Andrey Novitsky, Cheng-Wei Qiu, and Haifeng Wang, Single gradientless light beam drags particles as tractor beams, Phys. Rev. Lett. **107**, 203601 (2011).
[3] Florian O. Fahrbach, Philipp Simon, and Alexander Rohrbach, Microscopy with self-reconstructing beams, Nat. Photonics **4**, 780 (2010).
[4] Marti Duocastella and Craig B. Arnold, Bessel and annular beams for materials processing, Laser Photonics Rev. **6**, 607 (2012).
[5] Ralf Dorn, S. Quabis, and G. Leuchs, Sharper focus for a radially polarized light beam, Phys. Rev. Lett. **91**, 233901 (2003).
[6] Qiwen Zhan, Cylindrical vector beams: From mathematical concepts to applications, Adv. Opt. Photonics **1**, 1 (2009).
[7] J. Durnin, J. J. Miceli, and J. H. Eberly, Diffraction-free beams, Phys. Rev. Lett. **58**, 1499 (1987).
[8] N. Yu and F. Capasso, Flat optics with designer metasurfaces, Nat. Mater. **13**, 139 (2014).
[9] A. V. Kildishev, A. Boltasseva, and V. M. Shalaev, Planar photonics with metasurfaces, Science **339**, 1232009 (2013).
[10] C. L. Holloway, E. F. Kuester, J. A. Gordon, J. O'Hara, J. Booth, and D. R. Smith, An overview of the theory and applications of metasurfaces: The two-dimensional equivalents of metamaterials, IEEE Antennas Propag. Mag. **54**, 10 (2012).
[11] N. Yu, P. Genevet, M. A. Kats, F. Aieta, J. P. Tetienne, F. Capasso, and Z. Gaburro, Light propagation with phase discontinuities: Generalized laws of reflection and refraction, Science **334**, 333 (2011).
[12] Francesco Aieta, Patrice Genevet, Mikhail A. Kats, Nanfang Yu, Romain Blanchard, Zeno Gaburro, and Federico Capasso, Aberration-free ultrathin flat lenses and axicons at telecom wavelengths based on plasmonic metasurfaces, Nano Lett. **12**, 4932 (2012).
[13] Xingjie Ni, Satoshi Ishii, Alexander V. Kildishev, and Vladimir M. Shalaev, Ultra-thin, planar, babinet-inverted plasmonic metalenses, Light Sci. Appl. **2**, e72 (2013).
[14] C. Pfeiffer and A. Grbic, Metamaterial Huygens' surfaces: Tailoring wave fronts with reflectionless sheets, Phys. Rev. Lett. **110**, 197401 (2013).
[15] Jiao Lin, Patrice Genevet, Mikhail A. Kats, Nicholas Antoniou, and Federico Capasso, Nanostructured holograms for broadband manipulation of vector beams, Nano Lett. **13**, 4269 (2013).

[16] Nicolas Gagnon, Aldo Petosa, and Derek A. McNamara, Research and development on phase-shifting surfaces (PSSs), IEEE Antennas Propag. Mag. **55**, 29 (2013).
[17] Qiwen Zhan and James Leger, Focus shaping using cylindrical vector beams, Opt. Express **10**, 324 (2002).
[18] J. Durnin, Exact solutions for nondiffracting beams. I. The scalar theory, J. Opt. Soc. Am. A **4**, 651 (1987).
[19] S. R. Mishra, A vector wave analysis of a Bessel beam, Opt. Commun. **85**, 159 (1991).
[20] Martynas Beresna, Mindaugas Gecevičius, Peter G. Kazansky, and Titas Gertus, Radially polarized optical vortex converter created by femtosecond laser nanostructuring of glass, Appl. Phys. Lett. **98**, 201101 (2011).
[21] G. Machavariani, Y. Lumer, I. Moshe, A. Meir, and S. Jackel, Spatially-variable retardation plate for efficient generation of radially- and azimuthally-polarized beams, Opt. Commun. **281**, 732 (2008).
[22] Lingling Huang, Xianzhong Chen, Holger Muhlenbernd, Guixin Li, Benfeng Bai, Qiaofeng Tan, Guofan Jin, Thomas Zentgraf, and Shuang Zhang, Dispersionless phase discontinuities for controlling light propagation, Nano Lett. **12**, 5750 (2012).
[23] See Supplemental Material at http://link.aps.org/supplemental/10.1103/PhysRevApplied.2.044012 for additional information on the measurement and design of the metasurfaces.
[24] C. Pfeiffer and A. Grbic, Millimeter-wave transmitarrays for wavefront and polarization control, IEEE Trans. Microwave Theory Tech. **61**, 4407 (2013).
[25] F. Monticone, N. M. Estakhri, and A. Alù, Full control of nanoscale optical transmission with a composite metascreen, Phys. Rev. Lett. **110**, 203903 (2013).
[26] C. Pfeiffer and A. Grbic, Cascaded metasurfaces for complete phase and polarization control, Appl. Phys. Lett. **102**, 231116 (2013).
[27] P. F. Goldsmith, Quasi-optical techniques, Proc. IEEE **80**, 1729 (1992).
[28] Mauro Ettorre and Anthony Grbic, Generation of propagating Bessel beams using leaky-wave modes, IEEE Trans. Antennas Propag. **60**, 3605 (2012).
[29] Mauro Ettorre, Scott Michael Rudolph, and Anthony Grbic, Generation of propagating Bessel beams using leaky-wave modes: Experimental validation, IEEE Trans. Antennas Propag. **60**, 2645 (2012).
[30] Constantine A. Balanis, *Antenna Theory: Analysis and Design* (Wiley, New York, 2012).
[31] Makoto Ando, Kimio Sakurai, Naohisa Goto, Kunitaka Arimura, and Yoshiharu Ito, A radial line slot antenna for 12 GHz satellite TV reception, IEEE Trans. Antennas Propag. **33**, 1347 (1985).
[32] Jose I. Herranz-Herruzo, Alejandro Valero-Nogueira, and Miguel Ferrando-Bataller, Optimization technique for linearly polarized radial-line slot-array antennas using the multiple sweep method of moments, IEEE Trans. Antennas Propag. **52**, 1015 (2004).
[33] A. P. Feresidis and J. C. Vardaxoglou, High gain planar antenna using optimised partially reflective surfaces, IEE Proc. Microwaves Antennas Propagation **148**, 345 (2001).
[34] Arthur A. Oliner and David R. Jackson, *Antenna Engineering Handbook* (McGraw-Hill, New York, 2007), Vol. 4, Chap. 11.
[35] Gabriele Minatti, Francesco Caminita, Massimiliano Casaletti, and Stefano Maci, Spiral leaky-wave antennas based on modulated surface impedance, IEEE Trans. Antennas Propag. **59**, 4436 (2011).
[36] Carl Pfeiffer and Anthony Grbic, Bianisotropic metasurfaces for optimal polarization control: Analysis and synthesis, preceding paper, Phys. Rev. Applied **2**, 044011 (2014).
[37] Ashkan Vakil and Nader Engheta, Transformation optics using graphene, Science **332**, 1291 (2011).
[38] Paloma A. Huidobro, Maxim L. Nesterov, Luis Martin-Moreno, and Francisco J. Garcia-Vidal, Transformation optics for plasmonics, Nano Lett. **10**, 1985 (2010).
[39] Shulin Sun, Qiong He, Shiyi Xiao, Qin Xu, Xin Li, and Lei Zhou, Gradient-index meta-surfaces as a bridge linking propagating waves and surface waves, Nat. Mater. **11**, 426 (2012).
[40] Carl Pfeiffer, Naresh Kumar Emani, Amr M. Shaltout, Alexandra Boltasseva, Vladimir M. Shalaev, and Anthony Grbic, Efficient light bending with isotropic metamaterial Huygens' surfaces, Nano Lett. **14**, 2491 (2014).
[41] Y. Zhao, M. A. Belkin, and A. Alù, Twisted optical metamaterials for planarized ultrathin broadband circular polarizers, Nat. Commun. **3**, 870 (2012).